Available online at www.sciencedirect.com
ScienceDirect
Journal of Crystal Growth 310 (2008) 1355–1361
JOURNAL OF CRYSTAL GROWTH
www.elsevier.com/locate/jcrysgro

# Correlation between thermal parameters, structures, dendritic spacing and corrosion behavior of Zn–Al alloys with columnar to equiaxed transition

A.E. Ares[a,b,*], L.M. Gassa[c], S.F. Gueijman[b], C.E. Schvezov[a,b]

[a]*CONICET, Argentina*
[b]*University of Misiones, 1552 Félix de Azara Street, 3300 Posadas-Misiones, Argentina*
[c]*CONICET-INIFTA (Instituto de Investigaciones Fisicoquímicas Teóricas y Aplicadas), Universidad Nacional de la Plata, Diagonal 113 y 64, La Plata, Argentina*

Available online 4 December 2007

**Abstract**

The columnar to equiaxed transition (CET) has been examined for many years and the significance of CET has been treated in several articles. Experimental observations in different alloy systems have shown that the position of the transition is dependent on parameters like cooling rate, velocity of the liquidus and solidus fronts, local solidification time, temperature gradients and recalescence. The dendritic structure in alloys results in microsegregation of solute species which affects significantly the mechanical properties of the material. The main parameters characterizing the microstructure and the length range of microsegregation is the spacing which is classified as primary, secondary and tertiary. Properties like mechanical resistance and ductility are influenced by the dimensions and continuity of the primary branches, while the secondary and tertiary branches permit the isolation of interdendritic phases which can deteriorate the mechanical behavior of the material. Since the morphology and dimensions of the dendritic structure is related to the solidification parameters mentioned above, for each type of alloy it is essential to correlate dimensions and solidification conditions in order to control the structure. The objective of the present research consists on studying the influence of solidification thermal parameters with the type of structure (columnar, equiaxial or with the CET); and with grain size and dendritic spacing (primary and secondary) in Zn–Al (ZA) alloys (Zn—4 wt%Al, Zn—16 wt%Al and Zn—27 wt%Al, weight percent). Also, correlate the thermal parameters, type of structure, grain size and dendritic spacing with the corrosion resistance of these alloys.


*PACS:* 61.82.Bg; 81.10.Fq; 81.30.Fb; 81.40.−z; 82.45.Bb; 81.70.−q

*Keywords:* A1. Columnar to equiaxed transition; A1. Dendrites; A1. Directional solidification; A2. Growth from melt; A3. Electrochemical characterization; B1. Alloys

## 1. Introduction

Among the group of zinc base alloys (ZA4, ZA8, ZA12, ZA27), the zinc–aluminum alloys (ZA or ALZEN) have gotten a lot of attention in the last years like substitute materials of aluminum base alloys, irons and brasses [1].

The ZA27 alloy (ASTM B669–82, 25–28%Al, 2.0–2.5%Cu, 0.01–0.02%Mg and Zn-balance) has a higher mechanical resistance, ductility and resistance to abrasive wear of the group [2].

In general, equiaxed grains grow ahead of the columnar dendrites and the columnar to equiaxed transition (CET) occurs when these equiaxed grains are sufficient in size and number to impede the advance of the columnar front. The authors determined in a previous research that the extent of the equiaxed zone is the result of competition between the columnar and the equiaxed grains [3–5]. Spittle recently

*Corresponding author. University of Misiones, 1552 Félix de Azara Street, 3300 Posadas-Misiones, Argentina. Tel.: +54 3752 434118; fax: +54 3752425414.
*E-mail address:* aares@fceqyn.unam.edu.ar (A.E. Ares).

0022-0248/$ - see front matter © 2007 Elsevier B.V. All rights reserved.
doi:10.1016/j.jcrysgro.2007.11.169

summarized and assessed the present level of understanding of the CET [6].

In the industrial production it is very important to increase the quantity of quality products and without defects, where the structural morphology can also play an important role in the corrosion behavior of the metallic alloys. Although it is well-known that, as much the quantity as the homogeneity in the distribution of second phases are important parameters that define the level of mechanical resistance of the alloys [7–11]. It is necessary to study in systematic form the relation between the thermal and structural parameters and the resistance to the corrosion.

Recently, Song et al. [12] and Osório et al. [13–16] have reported a direct correlation between the tensile yield strength and the corrosion resistance of AZ91D alloys, Zn–Al alloys, Al–Si alloys, Al–9%Si and Al–20%Sn alloys.

The results presented in this paper focus on the CET studies in ZA4, ZA16 and ZA27 alloys. In the investigation, we correlate the effect of several parameters, like thermal, structural and electrochemical parameters on the transition and the type of structure.

In order to obtain the CET, the alloys were solidified directionally upwards in an experimental set up consisting of a heating unit, a temperature control system, a temperature data acquisition system, a sample moving system and a heat extraction system, with a set of thermocouples in the samples which permit to determine the time dependent profiles during growth. From these profiles and the location of thermocouples it was possible to calculate the cooling rates, growth velocities and the temperature gradients along the sample.

The primary and secondary spacings were measured and correlated with the solidification parameters. The corrosion study was realized by electrochemical impedance spectroscopy and polarization curves. The CET zone and the equiaxed structures presented a better corrosion resistance than the columnar zone.

## 2. Experimental procedure

ZA alloys of different compositions were prepared from zinc (99.998%) and aluminum (99.960%). The samples were directional solidified in alumina molds of 16.00 mm in diameter and 200 mm in length.

The alloy samples were melted and solidified directionally upwards in an experimental set up described elsewhere [3–5].

During the solidification process, temperatures at different positions in the alloy samples were automatically acquired using a data logger. The temperature measurements were performed using five K-type thermocouples (2 mm), which were protected with a refractory paste.

After solidification the samples were cut in the axial direction, were polished and the zinc–aluminum alloys were etched using concentrated hydrochloric acid for 3 s at room temperature, followed by rinsing and wiping off the resulting black deposit and for microstructures were etched with a mix containing chromic acid (50 g $Cr_2O_3$; 4 g $Na_2SO_4$ in 100 ml of water) for 10 s at room temperature [17]. Typical macrostructure and microstructures are shown in Fig. 1. The position of the transition was located by visual observation and optical microscopy and the distance from the chill zone of the sample was measured with a ruler. It is noted in Fig. 1(a) that the melted zone in the experiment starts at the region marked as zero on the macrostructure and the CET is not sharp, showing a zone where some equiaxed grains co-exist with columnar grains. The size of the transition zone is in the order of up to 10 mm. As previously reported [3,5] no effect of the set of the thermocouples in the transition was observed; either acting as nucleating sites or changing the solidification structure.

The equiaxed grain size is measured using the ASTM standard norm [18], at equally spaced intervals. The procedure for the columnar grains was as followed; the width was determined dividing the number of grains per unit length in the whole sample width. The columnar length was defined for all the grains in the longitudinal section and averaged.

The range of growth velocity and temperature gradients employed in the experiments were 0.10–0.28 cm/s and 1–20 °C/cm, respectively.

The correlation between the different dendrite spacings and the parameters were determined by measuring the spacings in the regions close to the position of the thermocouples. The microstructure was inspected by employing optical microscopy and using an image processing systems Neophot 32 and Leica Quantimet 500 MC. The spacings were measured by counting the number of branches; primary ($\lambda_1$) or secondary ($\lambda_2$) along a line of known length. The mean value of $\lambda_1$ and $\lambda_2$ was calculated from 15 measurements in each zone. In order to find the possible transformations taking place during solidification and to correctly determine the beginning and the end of the solidification, a DSC analysis was utilized.

For the electrochemical tests (polarization curves and electrochemical impedance spectroscopy technique, EIS), samples of 2 cm in length of each zone (columnar, equiaxed and CET) and for each concentration, were prepared as working electrodes cutting from the longitudinal sections, polished with sandpaper (from CSi #200 until #1200) and washed with desmineralized water and dried by natural flow of air.

All the electrochemical tests were conducted in a 300 ml of a 3% NaCl solution at room temperature using an IM6d ZAHNER® electrik potentiostat coupled to a frequency analyzer system, a glass corrosion cell kit with a platinum counter electrode and a sutured calomel reference electrode (SCE).

Polarization curves were obtained using a scanning rate in the range of $0.002\,\mathrm{V/s} \leqslant v \leqslant 0.250\,\mathrm{V/s}$ from open circuit potential until to 0.250 V. Impedance spectrums were registered in the frequency range of $10^{-3}\,\mathrm{Hz} \leqslant f \leqslant 105\,\mathrm{Hz}$ in open circuit.

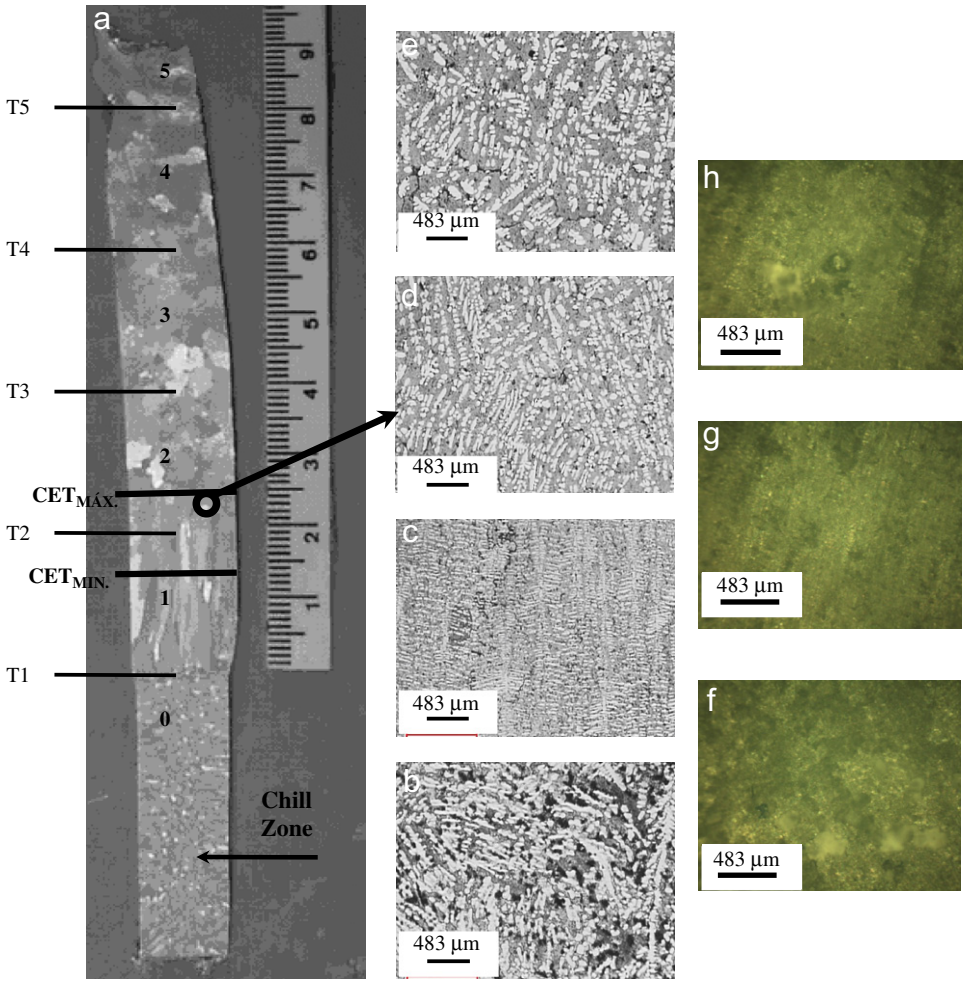


Fig. 1. (a) Macrostructure of a ZA4 alloy sample. It is indicated the position of thermocouples (T1–T5) and the sections between thermocouples (0–5). Also, in Figs. 1(b)–(e), representative microstructures are shown of each section, showing chill, columnar and equiaxed dendrite zones and the dendrites in the CET zone (Section 2). In Figs. 1(f)–(h), micrographs are presented after impedance test showing white deposit on the columnar electrode surface, indicating that the columnar structure is more susceptible to corrosion. (g) Relatively clean surface electrode of CET zone after EIS test.

## 3. Results and discussion

### 3.1. CET determinations

For the present research, a number of nine experiments in a range of alloys compositions and cooling rates were performed. The compositions cover a range; from 4 to 27 wt% Al for ZA alloys. Typical results of the transition are shown in Fig. 1 for Zn—4 wt%Al.

The transition is not sharp, showing a zone where some equiaxed grains co-exist with columnar grains. The size of the transition zone is in the order of up to 1 cm between the minimum position of the CET ($CET_{MIN}$) and the maximum position of the CET ($CET_{MAX}$).

In Fig. 1(a), it can be seen the macrostructure of a ZA4 alloy sample. It is indicated the position of thermocouples (T1–T5) and the sections between thermocouples (0–5). Also, in Figs. 1(b)–(e), representative microstructures are shown of each section, showing chill, columnar and equiaxed dendrite zones and the dendrites in the CET zone (Section 2). In Figs. 1(f)–(h), micrographs are presented after impedance test showing white deposit on the columnar electrode surface, indicating that the columnar structure is more susceptible to corrosion. (g) Relatively clean surface electrode of CET zone after EIS test.

### 3.2. Temperature measurements

A typical time dependent temperature plot for the all thermocouples in a sample with CET is shown in Fig. 2 for Zn—4 wt%Al alloy.

The thermocouple $T_1$ is at the lowest position and the first to reach the solidification front and $T_5$ is at the highest position. In all the curves it is possible to identify a period corresponding to the cooling of the melt, a second period of solidification and the final period of cooling of the solid to ambient temperature. In some particular cases, it is possible to identify a short period of recalescence, when the CET occurs at a given thermocouple position.

### 3.3. Solidification parameters

From the data shown in Fig. 2, the following information can be extracted; melt superheat, cooling rate of the melt, position of the solidification fronts for the solidus and the liquidus temperature, local solidification time, velocity of solidification fronts, length of the mushy zone, cooling rate of the solid and temperature gradients.

In some cases the quantification of these parameters is straightforward like the case of melt superheat, which is the highest temperature above the liquidus reached by the melt before the furnace is turned off. It is also the case of cooling rate, $\dot{T}$, which is calculated as the slope of the temperature curve in both periods, the cooling of the melt and the solid.

The start and the end of solidification at each thermocouple determine the positions of the solidification fronts versus time, which correspond to the experimental liquidus, $T_L$, and solidus, $T_S$, temperature, respectively, these are not necessarily the liquidus and the solidus temperature from the equilibrium phase diagram. Both points are detected by changes in slopes of the cooling curves at the start and at the end of solidification. This criterion was chosen in order to allow for undercooling to occur before solidification and possible recalescence during solidification of equiaxed grains, since this process is characterized by nucleation and solidification of grains in the melt rather than for what is observed in a normal solidification process where there is a dendrite tip front advancing in the melt. The local solidification time, $t_{LS}$, at each thermocouple location is determined by the period of time taken for the temperature going from the liquidus to the solidus temperature.

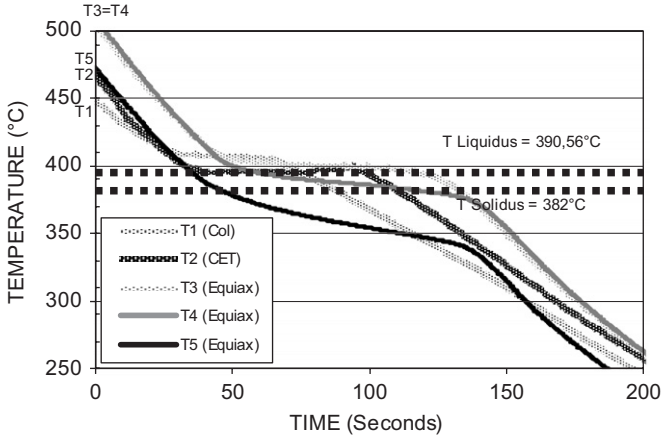


Fig. 2. Temperature versus time dependence. Zn—4 wt%Al alloy.

The velocity of a given solidification front is calculated as the distance between the thermocouples divided by the time taken by either, the liquidus or solidus temperature to go from the lower to the upper thermocouple. These velocities are named as $v_L$ and $v_S$ for the liquidus and solidus velocity, respectively.

The temperature gradients, $G$, at all times are calculated straightforward, dividing the temperature difference between two thermocouples by the separation distance between them.

The more important thermal parameters extracted from the nine experiments are presented in Table 1.

### 3.4. Grain size measurements

From a typical histogram showing the frequency of the size of the equiaxed grains for each and all the size intervals the equiaxed grain size was determined [3,5,18]. The results, which also include the width of the columnar grain, are plotted as function of position in the solidified sample for one sample in Fig. 3.

In Fig. 3, the size of the equiaxed grains is 0.3 mm in the transition region and then starts to monotonically increase to a value of 1.5 mm at the end of the sample and part of the alloy that solidified last. In the case of the width of the columnar grains it is observed that they are constant in size at the transition region (1 mm). Similar analyses were realized in the other alloy samples (Fig. 2).

### 3.5. Primary dendritic spacing measurements

The primary spacing ($\lambda_1$) for three different alloys was analyzed as a function of distance from the base of the

Table 1
Liquidus temperature ($T_L$), solidus temperature ($T_S$), average cooling rate of the melt ($\dot{T}_{average}$), critical liquidus interface velocity ($V_{LC}$), average position of the CET ($CET_{average}$), between the minimum position ($CET_{MIN}$) and the maximum position ($CET_{MAX}$) and critical gradients ($G_C$) obtained from temperature versus time curves for each alloy system

| No. | Alloy | $T_L$ (°C) | $T_S$ (°C) | $\dot{T}_{average}$ (°C/s) | $V_{LC}$ (cm/s) | $CET_{average}$ (cm) | $G_{critical}$ (°C/cm) |
|---|---|---|---|---|---|---|---|
| 1 | Zn—4 wt%Al | 390.56 | 382.00 | 1.77 | 0.16 | 2.2 | −0.49 |
| 2 | Zn—4 wt%Al | 390.56 | 382.00 | 2.21 | 0.28 | 5.0 | −0.31 |
| 3 | Zn—4 wt%Al | 390.56 | 382.00 | 2.63 | 0.10 | 7.2 | −0.09 |
| 4 | Zn—16 wt%Al | 462.01 | 382.00 | 2.18 | 0.16 | 1.7 | 1.67 |
| 5 | Zn—16 wt%Al | 462.01 | 382.00 | 3.78 | 0.17 | 3.3 | −0.46 |
| 6 | Zn—16 wt%Al | 462.01 | 382.00 | 2.84 | 0.18 | 2.5 | −2.1 |
| 7 | Zn—27 wt%Al | 505.00 | 275.00 | 2.43 | 0.15 | 3.3 | −1.25 |
| 8 | Zn—27 wt%Al | 505.00 | 275.00 | 2.15 | 0.21 | 2.3 | 0.55 |
| 9 | Zn—27 wt%Al | 505.00 | 275.00 | 3.5 | 0.19 | 5.2 | −0.68 |

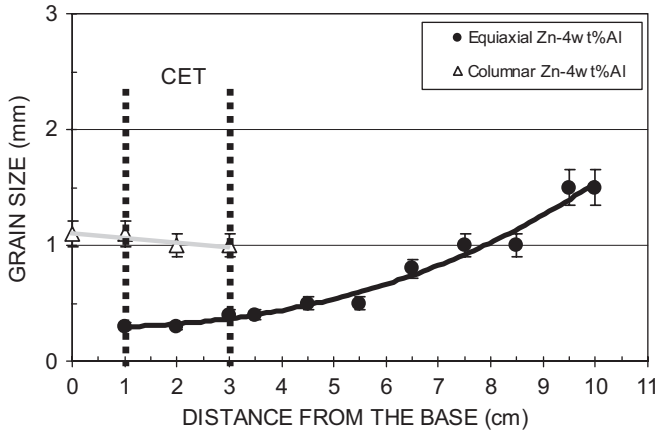


Fig. 3. Grain size versus distance from the base of the sample. Zn—4 wt%Al alloy.

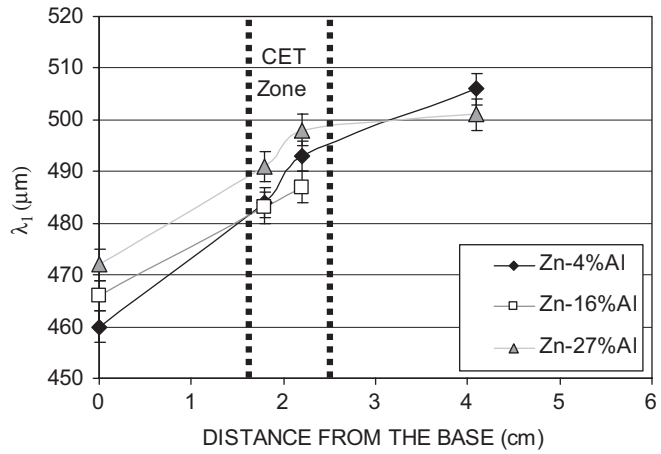


Fig. 4. Primary dendritic arm spacing versus distance from the base for different ZA alloys with approximately similar CET region.

sample. It must be noted that the solidification conditions changed along the sample producing structures which may change from columnar to equiaxed growth.

The primary dendritic arm spacing versus distance from the base for different ZA alloys with approximately similar size of the CET region is presented in Fig. 4; the error in the measurements is indicated in the same figure. It is observed that the spacing steadily increases with distance from the bottom and rapidly increases at the top where there is a transition from columnar to equiaxed; however, this last structure is not fully developed.

Similar results were obtained for Zn—16 wt%Al and Zn—27 wt%Al alloys with spacings of 460–490 μm in the columnar zone, up to 480 μm in the transition zone and up to 505 μm in the equiaxed grains.

The increase in $\lambda_1$ spacing from the chill zone of the sample is due to the corresponding decrease in cooling rate, $\dot{T}$. It is observed that in three cases the primary arm spacing increases steadily in the columnar zone with a peak in the columnar to equiaxed region; then the spacing increases steadily in the equiaxed region or become constant. Comparing the effect of alloying element, for columnar growth the primary spacing decreases with the Al concentration. The relation become less clear in the transition zone and becomes inverse in the equiaxed region. This behavior could be attributed to local effects since the solidification direction is random.

### 3.6. Secondary dendritic spacing measurements

In addition, the secondary arm spacing ($\lambda_2$) was plotted as a function of distance from the bottom of the sample for Zn—4 wt%Al, Zn—16 wt%Al and Zn—27 wt%Al alloys in Fig. 5. The increase of secondary spacing is strictly related to the increase in local solidification time for one specific alloy [19,20]. In the present experiments as shown by the temperature readings the solidification time increases from the start of solidification towards the end at the top, as the macrostructure changes from columnar to equiaxed. The increase in solidification time is produced by a larger acceleration of the liquidus interface [3,5] with respect to the solidus interface. This acceleration is believed to be produced by the fast nucleation of the equiaxed grains after the start of the CET.

On the other hand, increasing the aluminum content of the alloy according to the binary phase diagram naturally increases the difference between $T_L$ and $T_S$ which in turn, increases the local solidification time for similar cooling rates.

### 3.7. Electrochemical parameters

From the analysis of the currents of peaks in the obtained polarization curves, it is possible to appreciate that the columnar structure is the most susceptible to the corrosion, fundamentally in the case of the alloy with only 4 wt% of Al.

The rest of the structures presented currents of peaks in the same order, independently to the concentration of Al present in the alloy. In Fig. 6 are presented, as an example, voltammograms corresponding to Zn—4 wt%Al,

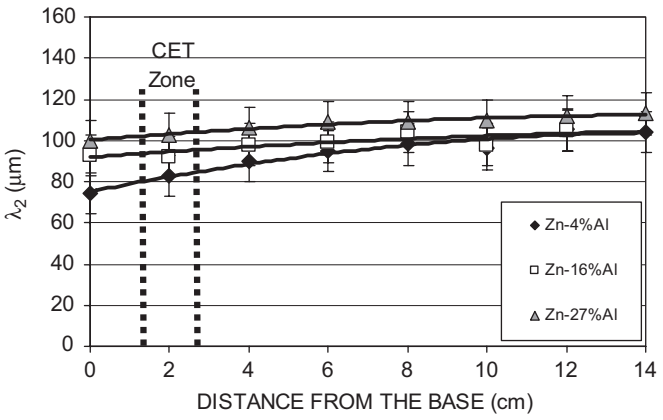


Fig. 5. Secondary dendritic arm spacing versus distance from the base for different ZA alloys.

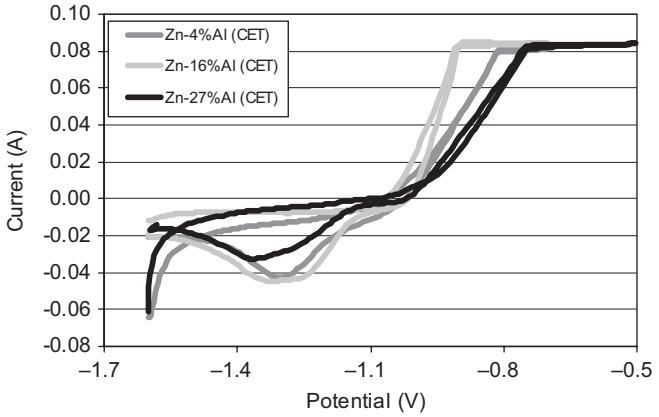


Fig. 6. Voltammograms of CET zones for different ZA alloys.

Table 2
Principal parameters obtained from the EIS analysis

| Alloy sample | $R_\Omega$ ($\Omega$ cm$^2$) | $C_{dl}$ (F/cm$^2$) | $R_{ct}$ ($\Omega$ cm$^2$) |
|---|---|---|---|
| Zn—4%Al$_{columnar}$ | 32 | $2.6\times10^{-4}$ | 23.07 |
| Zn—4%Al$_{CET}$ | 35.4 | $1.6\times10^{-6}$ | 1785.68 |
| Zn—4%Al$_{equiaxial}$ | 816.2 | $2.1\times10^{-6}$ | $3727\times10^{5}$ |
| Zn—16%Al$_{columnar}$ | 20.88 | $3.2\times10^{-4}$ | 124.33 |
| Zn—16%Al$_{CET}$ | 60.36 | $1.2\times10^{-4}$ | 34.17 |
| Zn—16%Al$_{equiaxial}$ | 30.58 | $1.57\times10^{-4}$ | 28.16 |
| Zn—27%Al$_{columnar}$ | 21.65 | $5.83\times10^{-4}$ | 179.91 |
| Zn—27%Al$_{CET}$ | 509.71 | $2.00\times10^{-6}$ | $215\times10^{6}$ |

Zn—16 wt%Al and Zn—27 wt%Al alloys in the CET zone of the samples.

The impedance diagrams showed only one capacitive time constant and they were adjusted with the following function of transference:

$$Z_t(j\omega) = R_\Omega + Z, \quad (1)$$

where $Z = R_{ct} + (1/j\omega C_{dl})$, $\omega = 2\pi f$, $R_\Omega$ is the Ohmic solution resistance and $C_{dl}$ is the differential capacitance of the electric double layer.

In Table 2 are presenting the values of the adjusting parameters for each zone and alloy concentration. In Zn—4 wt%Al and Zn—27 wt%Al the corrosion susceptibility depends on the structure of the alloy. In Figs. 1(e)–(g), micrographs are presented with different structures of Zn—4 wt%Al alloy after the impedance test showing white deposit on the columnar surface of the electrode, showing that columnar structure is more susceptible to corrosion and a relatively clean electrode surface of the CET zone after EIS test. The alloy with 16 wt%Al is the less resistant to the corrosion and their susceptibility to the corrosion is independent of the structure. The alloy with 27 wt%Al and CET structure is the most resistant of all. In Fig. 7 are presented the experimental and fitted Bode diagrams in the CET zone of the sample of Zn—4 wt%Al alloy. In this figure it is possible to appreciate the good agreement between experimental results and calculated data using non-linear fit routines according to the corresponding transfer function at the different operational potentials.

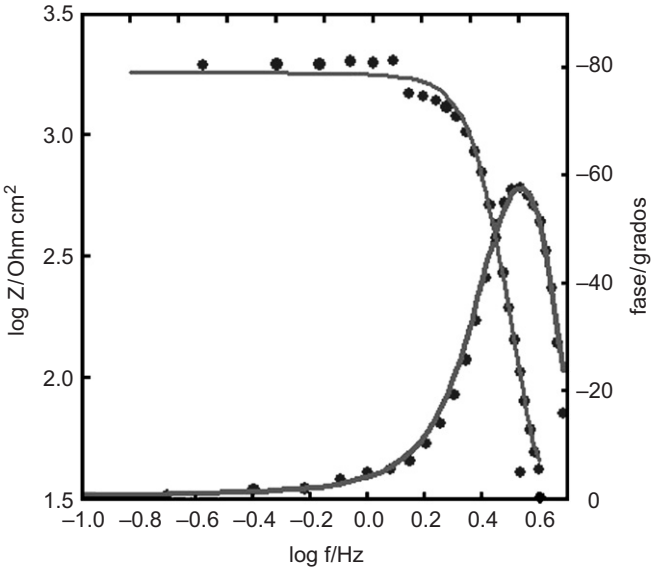


Fig. 7. Bode diagram of CET zone for Zn—4 wt%Al alloy sample.

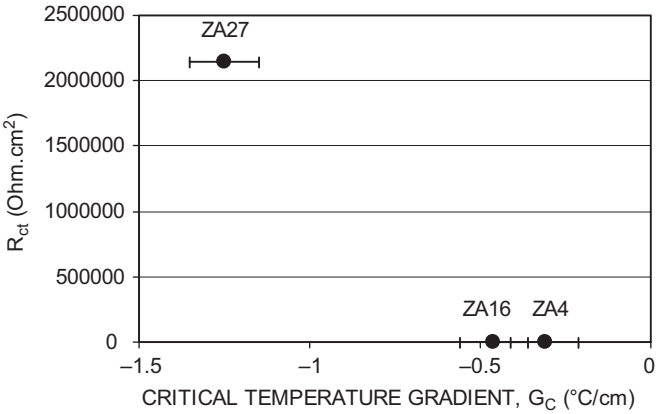


Fig. 8. Correlation of $R_{ct}$ with temperature gradient at the moment of the CET, $G_C$.

In the case of Zn—27 wt%Al$_{equiaxial}$ alloy, and due to the high susceptibility to the corrosion of that alloy, the stationary state was not reached to apply the impedance technique.

### 3.8. Correlation between of electrochemical parameters with others parameters

The obtained values of the charge-transfer resistance, $R_{ct}$, were correlated with the values of temperature gradient in the liquid at the moment of the CET (critical values), $G_C$, for each concentration (see Fig. 8) and were obtained that, when $G_C$ become more negative, the $R_{ct}$ increase.

In the case of the correlation of the charge-transfer resistance with the structural parameters, that is with grain size and secondary dendritic spacing, were obtained that when both parameters increases, the charge-transfer

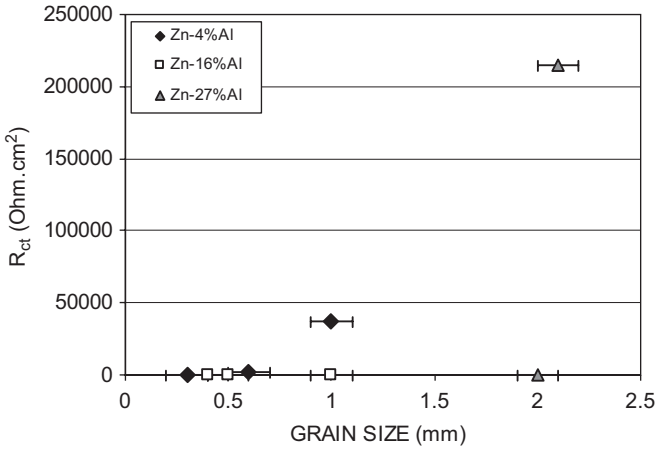


Fig. 9. Correlation of $R_{ct}$ with grain size.

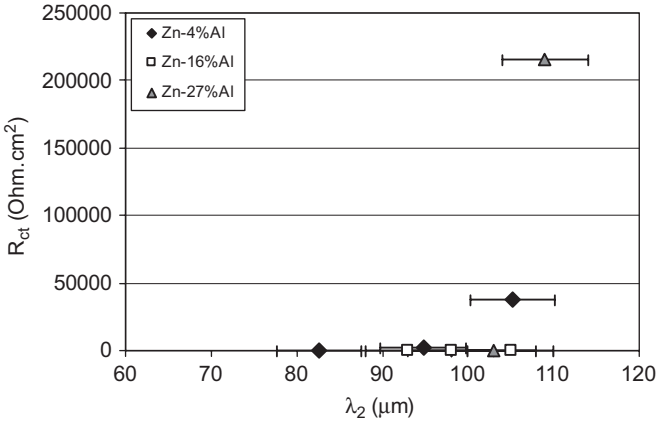


Fig. 10. Correlation of $R_{ct}$ with $\lambda_2$.

resistance also increased (see Figs. 9 and 10, respectively). This behavior not occurred for ZA16 alloy.

## 4. Conclusions

From the results and discussion of the previous sections the main conclusions of this investigation on the correlation between different parameters on the CET in Zn–Al alloys are:

1. ZA (Zn—4 wt%Al, Zn—16 wt%Al and Zn—27 wt%Al) alloys with different types of structures were obtained and the CET occurs in a zone rather than in a sharp plane, where both columnar and equiaxed grains in the melt co-exist.
2. The temperature gradient and the velocity of the liquidus front reach critical values at the CET.
3. The grain size is smaller at the CET region and then beginning to increases until the upper zone of the sample is reached.
4. The dendritic spacing increases with the Al content in the ZA alloys and from the columnar zone to equiaxed region due to the corresponding decreasing in cooling rate.
5. The polarization curves showed that the columnar structure is the most susceptible to the corrosion, fundamentally in the case of the alloy with only 4 wt% of Al. The rest of the structures presented currents of peaks in the same order, independently to the concentration of Al present in the alloy.
6. The biggest susceptibility to the corrosion of the alloys with columnar structure it is possible to observe analyzing the values of $R_{ct}$ obtained using the EIS technique. In Zn—4 wt%Al and Zn—27 wt%Al the corrosion susceptibility depends on the structure of the alloy. The alloy with 16 wt%Al is the less resistant to the corrosion and their susceptibility to the corrosion is independent of the structure. The alloy with 27 wt%Al and CET structure is the most resistant of all.
7. In order to correlate $R_{ct}$ with $G_C$, where obtained that, when $G_C$ become more negative, the $R_{ct}$ increase.
8. In the case of the correlation of the charge-transfer resistance with the structural parameters, that is with grain size and secondary dendritic spacing, when both parameters increased, the charge-transfer resistance also increased. This did not happen with ZA16 alloy.

## Acknowledgment

Thanks are given to the Argentinean Research Council (CONICET) for the financial support.

## References

[1] L.J. Yang, J. Mater. Process. Technol. 140 (2003) 391.
[2] Barnhurst, in: AFS Transaction, 1991, pp. 321–324.
[3] A.E. Ares, C.E. Schvezov, Metallurg. Mater. Trans. 31A (2000) 1611.
[4] A.E. Ares, S.F. Gueijman, C.E. Schvezov, J. Crystal Growth 241 (2002) 235.
[5] A.E. Ares, C.E. Schvezov, Metallurg. Mater. Trans. 38A (2007) 1485.
[6] J.E. Spittle, Int. Mater. Rev. 51 (2006) 247.
[7] U. Feurer, in: The Symposium on Quality Control of Engineering Alloys, Delft, 1977, p. 131.
[8] R. Trivedi, W. Kurz, Int. Mater. Rev. 39 (1994) 49.
[9] R.N. Grugel, J. Mater. Sci. 28 (1993) 677.
[10] J.D. Hunt, in: Solidification and Casting of Metals, The Metals Society, London, 1979, pp. 3–9.
[11] W.R. Osório, C.A. Santos, J.M.V. Quaresma, A. Garcia, J. Mater. Process. Technol. 143–144 (2003) 703.
[12] G. Song, A. Atrens, M. Dargusch, Corros. Sci. 41 (1998) 249.
[13] W.R. Osório, C.M. Freire, A. Garcia, J. Alloys Compd. 397 (2005) 179.
[14] W.R. Osório, J.E. Spinelli, N. Cheoung, A. Garcia, Mater. Sci. Eng. A 420 (2006) 179.
[15] W.R. Osório, P.R. Goulart, G.A. Santos, C.M. Neto, A. Garcia, Metallurg. Mater. Trans. A 37 (2006) 2525.
[16] W.R. Oscrio, N. Cheoung, J.E. Spinelli, P.R. Goulart, A. Garcia, J. Solid State Electrochem. 11 (2007) 1421.
[17] G.F. Vander Voort, in: Metallography Principles and Practice, ASM International, New York, 2000, pp. 528–761.
[18] H.E. Boyer, T.L.Gall, Metals Handbook, Desk ed., American Society for Metals, 1990, pp. 35-18–35-19.
[19] A.E. Ares, R. Caram, C.E. Schvezov, Rev. Matér. 9 (2004) 411.
[20] A.E. Ares, R. Caram, C.E. Schvezov, Rev. Ciencia Tecnol. 6 (2004) 47.